BJ www.biochemj.org

BJ Structure

Biochem. J. (2008) **414**, 375–381 (Printed in Great Britain) doi:10.1042/BJ20080889

online data

Structural and mechanistic insights into type II trypanosomatid tryparedoxin-dependent peroxidases

Magnus S. ALPHEY[1], Janine KÖNIG[1] and Alan H. FAIRLAMB[2]

Division of Biological Chemistry and Drug Discovery, College of Life Sciences, University of Dundee, Dundee DD1 5EH, Scotland, U.K.

*Tb*TDPX (*Trypanosoma brucei* tryparedoxin-dependent peroxidase) is a genetically validated drug target in the fight against African sleeping sickness. Despite its similarity to members of the GPX (glutathione peroxidase) family, *Tb*TDPX2 is functional as a monomer, lacks a selenocysteine residue and relies instead on peroxidatic and resolving cysteine residues for catalysis and uses tryparedoxin rather than glutathione as electron donor. Kinetic studies indicate a saturable Ping Pong mechanism, unlike selenium-dependent GPXs, which display infinite K_m and V_{max} values. The structure of the reduced enzyme at 2.1 Å (0.21 nm) resolution reveals that the catalytic thiol groups are widely separated [19 Å (0.19 nm)] and thus unable to form a disulphide bond without a large conformational change in the secondary-structure architecture, as reported for certain plant GPXs. A model of the oxidized enzyme structure is presented and the implications for small-molecule inhibition are discussed.

Key words: dithiol-dependent peroxidase, drug discovery, glutathione peroxidase, *Leishmania*, *Trypanosoma*, trypanothione.

INTRODUCTION

Human African trypanosomiasis (sleeping sickness) is responsible for an estimated 80000 new cases and 30000 deaths each year [1]. Current therapeutics against the protozoan parasite (*Trypanosoma brucei* sspp.) are inadequate and new drugs are urgently needed [2].

Much research has focussed on the unique thiol metabolism of trypanosomes, centred around the metabolite trypanothione [N^1,N^8-bis(glutathionyl)spermidine] [3]. The trypanothione peroxidase system prevents damage by oxidative stress by reduction of peroxides via NADPH, trypanothione reductase, trypanothione, TryX (tryparedoxin) and tryparedoxin peroxidase, a two-cysteine-residue-containing peroxiredoxin. All components of this cascade are essential for parasite survival [4–8].

Recently, a new member of this antioxidant defence system has been identified and characterized in *T. brucei* [9–11], *T. cruzi* [12] and *Leishmania major* [13]. These TDPXs (tryparedoxin-dependent peroxidases) show highest homology, among the mammalian proteins, with GPX4, the monomeric phospholipid GPX (glutathione peroxidase). However, glutathione is not a physiological substrate for these TDPXs, which use TryX, a thioredoxin-like protein, as an electron donor. Moreover, the active-site selenocysteine residue in GPXs is replaced by a cysteine residue for reduction of a broad range of hydroperoxides, including H_2O_2 and complex lipid hydroperoxides. A resolving cysteine residue missing in all human GPXs is essential for regeneration by TryX. The essentiality of TDPX in *T. brucei*, shown by RNA-interference studies [8], together with the different reaction mechanism from the mammalian GPX, suggest that TDPX could be a druggable target in these parasites.

There are three TDPXs in *T. brucei*, which are localized in the mitochondrion and the cytosol [10]. Apart from putative targeting sequences at the N- and C-termini, the core of these proteins is highly conserved. Previous studies have kinetically characterized a His_6 (*T. brucei* TDPX3)(hexahistidine)-tagged *Tb*TDPX3 that included the putative mitochondrial targeting sequence [9]. Here we have kinetically analysed the non-tagged and shorter recombinant *Tb*TDPX2 and compared the results with those obtained with *Tb*TDPX3. We report the first TDPX crystal structure from a trypanosomatid, the reduced form of *Tb*TDPX2 at 2.1 Å (1 Å = 0.1 nm), and present a model of the oxidized form that may assist in the future design of inhibitors against this target.

EXPERIMENTAL

Cloning, expression, purification and characterization

*Tb*TDPX2 from strain S427 was cloned into pET15b (Novagen), expressed in *Escherichia coli* BL21(DE3)pLysS and purified as the His_6-tagged protein essentially as described for *Lm*TDPX1 (*Leishmania major* TDPX1) [13].

The His_6 tag was removed with thrombin and the enzyme purified to homogeneity by chromatography on nickel–Sepharose, benzamidine–Sepharose and gel filtration in 50 mM Tris/HCl buffer, pH 8.0. Assay conditions were essentially as described in [9]. Briefly, peroxidase activity was measured in a total volume of 250 μl at 25 °C containing 100 mM Tris/HCl, pH 7.6, 5 mM EDTA, 250 μM NADPH, 5 units of *Tb* trypanothione reductase, 100 μM trypanothione disulphide, 5 to 12.5 μM *Tb* TryX, 0.2 μM *Tb*TDPX2 and 50–800 μM cumene hydroperoxide. Kinetic data were analysed as described in [13].

For crystallization, His_6-tagged protein was reduced with 50 mM dithiothreitol, concentrated (Vivaspin 20 protein concentrator; Sartorius) and applied to a Superdex S75 26/60 (GE Healthcare) column equilibrated with 10 mM Tris/HCl, pH 8.0. *Tb*TDPX2-containing fractions were combined, 10 mM

Abbreviations used: GPX, glutathione peroxidase; His_6, hexahistidine; *Lm*, *Leishmania major*; PEG, poly(ethylene glycol); *Pt*, *Populus trichocarpaxdeltoides* (hybrid poplar); r.m.s.d., root mean square deviation; *Tb*, *Trypanosoma brucei*; TDPX, tryparedoxin-dependent peroxidase; TryX, tryparedoxin.

[1] These authors contributed equally to this work.

[2] To whom correspondence should be addressed (email a.h.fairlamb@dundee.ac.uk).

The model co-ordinates and structure factors have been deposited with the RSCB PDB (Research Collaboratory for Structural Bioinformatics Protein Data Bank) under the accession code 2VUP.

dithiothreitol and 1 mM EDTA (final concns.) were added, and the protein was concentrated to 7.5 mg/ml before crystallization.

Crystallization, data collection, structure solution and refinement

Crystals of His_6-tagged *Tb*TDPX2 were grown by the hanging-drop method at 18 °C. Drops (1 μl) of protein (7.5 mg/ml) and reservoir solution {22 % (w/v) PEG [poly(ethylene glycol)] 3350 and 0.1 M Tris/HCl, pH 8.0} were assembled, and monoclinic crystals (1.0 mm × 0.05 mm × 0.05 mm) were allowed to grow overnight. Crystals were cryoprotected in 35 % PEG 3350 and 0.1 M Tris/HCl, pH 8.0, and flash-cooled in a stream of nitrogen at 103 K. Data were collected at the European Synchrotron Radiation Facility (Grenoble, France) on beamline ID14 EH4 using an ADSC QUANTUM Q315r CCD (charge-coupled device) detector and at a wavelength of 0.979 Å. A single crystal was used to collect 180° of data in seven batches, as it was translated along its length to avoid the effects of radiation damage. Data were processed and scaled using XDS (X-ray Detector Software) [14] and statistics are shown in Supplementary Table S1 at http://www.BiochemJ.org/bj/414/bj4140375add.htm. The crystals contained one molecule in the asymmetric unit, the space group was $P2_1$ with a Matthews coefficient of 2.2 Å^3/Da, and the solvent content was 44 %.

Potential structural homologue candidates were identified in the RSCB PDB (Research Collaboratory for Structural Bioinformatics Protein Data Bank). Chain A of structure 2P5Q, the reduced form of *Pt*GPX5 [*Populus trichocarpaxdeltoides* (hybrid poplar) GPX5] [15], showing a sequence identity of 52 %, was used for molecular replacement in MOLREP [16]. The solution from MOLREP underwent rigid body refinement followed by restrained refinement in REFMAC5 [17,18], giving an R_{factor} and R_{free} of 32 and 40 % respectively. Residues were mutated from the *Pt*GPX5 sequence to that of *Tb*TDPX2 using COOT [19], and further cycles of restrained refinement interspersed with electron-density inspection, manual model building and manipulation and water addition were performed with REFMAC5 and COOT. All residues fall into the preferred and allowed regions of the Ramachandran plot. Surface-charge representations were prepared and visualized using PDB2SQR [20], APBS [21] and PyMOL (DeLano Scientific LLC). Refinement statistics can be found in Supplementary Table S1.

Sequence and structural alignments and modelling

Structural and sequence homologues were found using DALI [22] and BLAST searches of the PDB and Swiss-Prot databases. Only one structure, 1GP1 (bovine erythrocyte GPX1; [23]) was returned by DALI as a structural homologue, with an r.m.s.d. (root mean square deviation) of 1.8 Å over 159 Cα-atoms. However, the BLAST search of the PDB revealed several members of the GPX family, which when overlaid using LSQMAN [24,25] gave r.m.s.d. values of between 1.0 Å and 1.4 Å over more than 120 Cα-atoms and sequence identities of between 29 and 52 %. SWISS-MODEL [25] was used to prepare a structural model of the oxidized form of *Tb*TDPX2 on the basis of the structure of oxidized *Pt*GPX5. The three-dimensional structures were visualized and analysed with COOT and PyMOL.

RESULTS AND DISCUSSION

Kinetic analysis

Previous kinetic analyses of His_6-tagged *Tb*TDPX3 [9] showed no saturation kinetics, in contrast with that of non-tagged *Lm*TDPX1 [13]. *Tb*TDPX3 has a putative N-terminal mitochondrial targeting sequence, which, together with the His_6 tag, might interfere with enzyme activity. Thus we chose to work with the shorter *Tb*TDPX2 (Figure 1). Three independent PCRs were performed using genomic DNA from *Tb* strain 427 as template. All clones analysed contained two point mutations at the DNA level (C233A and T246C) in comparison with *Tb*TDPX2 in the genome reference strain (gene *Tb*927.7.1130). C233A causes a mutation (T78N) at the amino acid level, and T246C is silent (Figure 1).

Recombinant protein was expressed in *E. coli* and purified to homogeneity with and without the N-terminal His_6 tag (Supplementary Figure S1A at http://www.BiochemJ.org/bj/414/bj4140375add.htm). SDS/PAGE analysis shows that non-tagged *Tb*TDPX2, which has a predicted molecular mass of 19 168 Da, runs as a monomer in both its reduced and oxidised forms (Supplementary Figure S1B). Additionally, analytical size-exclusion chromatography shows that both forms are eluted as single monomeric peaks with molecular masses of 19 600 and 25 400 Da for the reduced and oxidized proteins respectively (Supplementary Figure S1C). The minor size differences observed using both methods is likely to be a result of the conformational change predicted to occur between the reduced and oxidized states as outlined below.

Kinetic data for non-tagged *Tb*TDPX2 were obtained by varying hydroperoxide concentrations at several fixed TryX concentrations. Results were analysed by fitting individual data sets to the Michaelis–Menten equation to obtain V_{max}^{app} for each concentration of TryX (Figure 2A). A double-reciprocal plot of $1/V_{max}^{app}$ versus 1/[TryX] gave finite values for K_m and V_{max} (Figure 2B). Since the double-reciprocal transformations of the original data set were parallel, the entire data set was globally fitted by non-linear regression to the equation describing a Ping Pong mechanism (Figure 2C). Similar results were found by analysis of progress curves using the integrated Dalziel equation analysed as described for *Tb*TDPX3 [9] (Supplementary Figure S2 at http://www.BiochemJ.org/bj/414/bj4140375add.htm). The results of these analyses are summarized in Table 1 in comparison with published data for *Tb*TDPX3 and *Lm*TDPX1. The rate constants k_1 and k_2 for cumene hydroperoxide and TryX respectively are in reasonable agreement with those reported for *Tb*TDPX3 [11], except that our results are compatible with finite K_m values in the micromolar range rather than infinite ones. Nonetheless, the kinetic behaviour of *Tb*TDPX2 and *Tb*TDPX3 are broadly similar and thus the N-terminal His_6 tag and N-terminal extension present in *Tb*TDPX3 does not significantly perturb kinetic behaviour. Interestingly, *Lm*TDPX1 and *Tb*TDPX2 show similar catalytic-centre activity (k_{cat}) and K_m values for cumene hydroperoxide, but differ markedly in K_m values for TryX, which is at least ten times lower for *Lm*TDPX1.

Overall structure and comparisons

The crystal structure of *Tb*TDPX2 has been solved using data to 2.1 Å and displays the well-characterized thioredoxin fold [26,27]. The structure (Figure 3) is constructed around a seven-stranded twisted β-sheet with parallel (β3–β4–β5–β1) and antiparallel (β3–β6–β7) sections sharing β3. The sheet is flanked by three α-helices on one side (α1, α2 and α4) and one on the other (α3). The secondary structure begins with a loop of two 3_{10} helices (θ1 and θ2) separated by a β-hairpin (β1 and β2) followed by a β–α–β unit (β3–α1–β4). The model contains 163 residues from Ala^3 to Thr^{166}. The His_6-affinity tag, N-terminal residues 1 and 2, and C-terminal residues 167 to 169 could not be modelled, owing to weak electron density, suggesting a high level of flexibility in these regions.

A BLAST search with the sequence for *Tb*TDPX2 returned many homologues that can be grouped with those from other

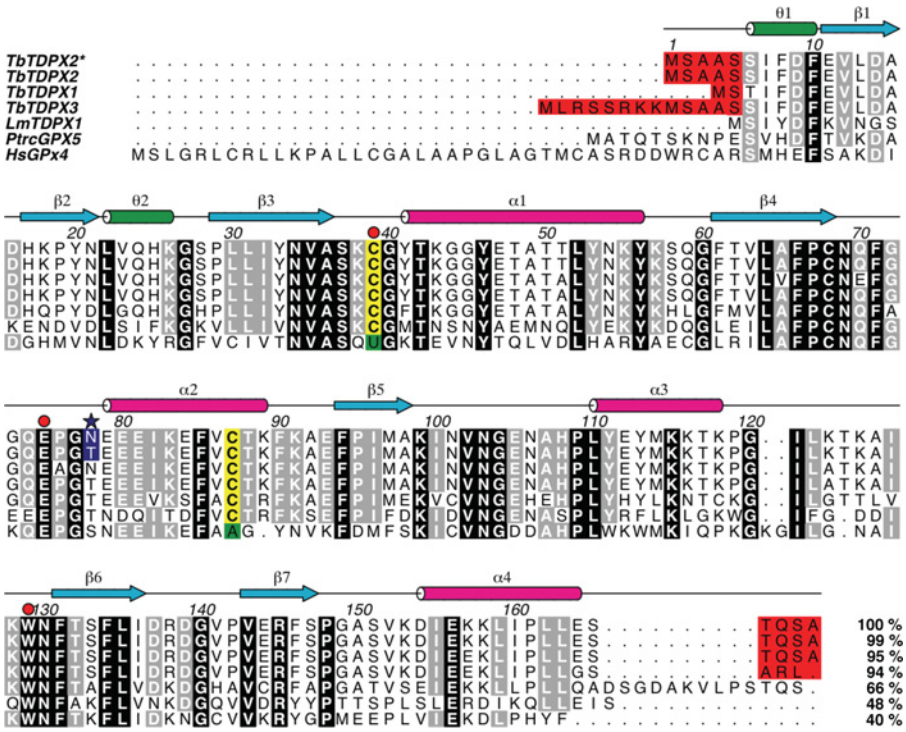

Figure 1 Sequence–structure alignment of TDPXs and homologues

The protein sequences are accessible in the Swiss-Prot/TrEMBL (translated EMBL) databank under the following accession numbers: *Tb*TDPX2 (Q869A6), *Tb*TDPX1 (Q869A7), *Tb*TDPX3 (Q869A5), *Lm*TDPX1 (Q4Q9B2), *Pt*GPX5 (A3FNZ8) and human GPX4 (P36969). Secondary-structure elements are colour-coded according to Figure 5, with α-helices in magenta, β-strands in cyan, and 3_{10}-helices in green. Residues identical in all sequences have been shaded in black, and those identical in most sequences are shaded in grey. Highlighted in yellow are the peroxidatic and resolving cysteine residues. The red circles denote the conserved active-site-triad residues. The different N- and C-termini of the three *Tb*TDPXs are shaded in red. The *Tb*TDPX2* sequence is that described in the present study, and the mutational difference from the database sequence is highlighted by the blue star. The numbers at the end of each sequence correspond to the percentage sequence identity with *Tb*TDPX2* in the alignment.

trypanosomes (~70 % identity), plants (~50 % identity) and animals (~30 % identity) (Figure 1). Only eight structural homologues were found in the Protein Data Bank: bovine erythrocyte GPX1 (1GP1), human GPX1, GPX2, GPX3, GPX4, GPX5 and GPX7 (2F8A, 2HE3, 2R37, 2OBI [28], 2I3Y and 2P31), and the two *Pt*GPX5 structures (2P5Q and 2P5R [15]). These structures were overlaid, revealing that the core subunit structures were well conserved, with r.m.s.d. values ranging from 1.0 Å over 155 Cα atoms for hGPX4, to 1.4 Å over 148 Cα atoms for hGPX3.

*Tb*TDPX2 exhibits strong similarities to the related GPXs. Unlike the majority of GPX structures that exist as either homodimers or homotetramers in solution, *Tb*TDPX2 exists as a monomer (Supplementary Figures S1B and S1C). Among the human GPXs, only hGPX4 is reported to be monomeric [28]. A minor deviation from the overlaid backbones is seen in loop α3–β6 of *Tb*TDPX2 (Figure 4). Although the conformation is slightly different in GPX4, this loop is the same length in both structures and shorter than the long surface-exposed loop seen in the other GPX isozymes. It has been suggested that the existence of the extended loop in other GPXs limits accessibility to the active site [28], and the short loop in hGPX4 and *Tb*TDPX2 may explain their broad substrate specificity. Two additional features of the *Tb*TDPX2 structure, α2 and the short loop α2–β5, share the same position as their equivalents in GPX4 (Figure 4), but, as can be seen in the oligomeric GPXs, these structural elements are involved in intersubunit interfaces and are therefore determinants of the oligomerization state of this family. Interestingly, in the monomeric *Tb*TDPX2, helix α2 contains the resolving Cys[87] as does the dimeric *Pt*GPX5. However, in *Pt*GPX5 the dimer interface is different to those formed by the oligomeric selenocysteine-containing mammalian GPXs, and so the resolving cysteine residue of *Pt*GPX5 is not constrained by the interface [15].

Bipartite active site

The active site of mammalian GPXs is comprised of a well-conserved cysteine, glutamine and tryptophan catalytic triad [23]. Mutational studies in *Tb*TDPX3 suggests that Cys[47] and Gln[82] (equivalent to Cys[39] and Gln[74] in *Tb*TDPX2) are essential for activity [11]. Mutation of Trp[137] to glycine, however, resulted in an enzyme with low, but significant, activity, suggesting that it plays a structural, rather than a catalytic, role [11]. Overlaying *Tb*TDPX2 with the other structurally described GPXs puts the triad components (Cys[39], Gln[74] and Trp[129]; Figure 5A) in similar positions, but in *Tb*TDPX2 the distance between the Cys[39] Sγ and Gln[74] Oε1 atoms is on average 0.4 Å greater than with the other homologues, whereas the distance between Cys[39] and the Trp[129] Nε1 atom is on average 0.5 Å shorter.

One of the most unusual features of the reduced form of *Tb*TDPX2 is that the peroxidatic Cys[39] and resolving Cys[87] are situated 19 Å away from each other (Figure 3) and reside in distinct environments. The peroxidatic Cys[39] is found in the loop connecting β3 and α1 and, although this loop is solvent-accessible, the side chain of Cys[39] points towards the molecule's interior, as seen in the reduced structure of *Pt*GPX5 [15]. Cys[39] is surrounded by Ala[36], Tyr[41], Gln[74], Trp[129], Asn[130] and Phe[131] that belong to loops β3–α1, β4–α2 and α3–β6 (Figure 5A). These

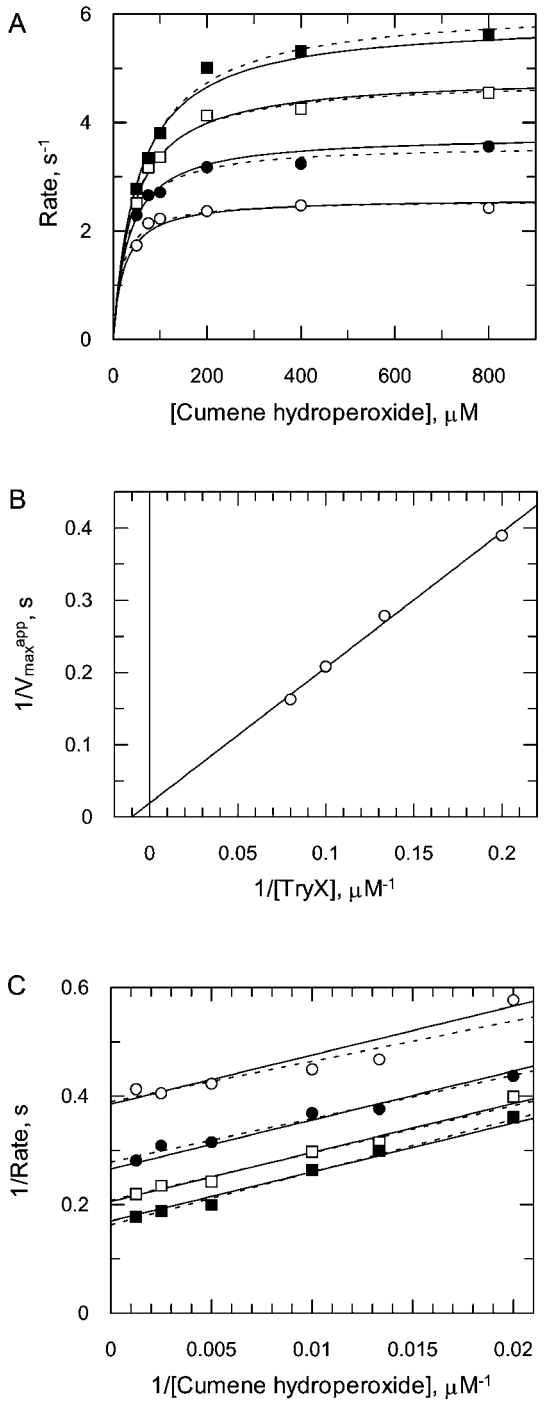

Figure 2 Kinetic analysis of TDPX2 with TryX and cumene hydroperoxide as substrate

(**A**) The initial velocities were determined with varied cumene hydroperoxide concentrations and different TryX concentrations (■, 12.5 μM; □, 10 μM; ●, 7.5 μM; ○, 5 μM). The initial velocities for each individual data set were initially fitted individually to the Michaelis–Menten equation (broken line) by non-linear regression using GraFit and subsequently the entire data set was globally fitted to the equation describing a Ping Pong mechanism (continuous line). (**B**) The reciprocal V_{max}^{app} data, calculated for each TryX concentration data set, were plotted against the reciprocal TryX concentrations. The reciprocal intercept represents the reciprocal V_{max} value and the reciprocal slope the rate constant k_2 for TryX. (**C**) The reciprocal initial velocities are plotted against the reciprocal cumene hydroperoxide concentrations. This Figure shows the accuracy of the two fits transformed as a Lineweaver–Burk plot (continuous line, global fit; broken line, individual fits for each TryX concentration). The slope represents the reciprocal rate constant, k_1, for cumene hydroperoxide. Kinetic constants are reported in Table 1.

Table 1 Kinetic properties of TDPX with TryX as reducing agent and cumene hydroperoxide as substrate

Data for *Tb*TDPX3 are from [9] and were fitted to the integrated Dalziel rate equation for a Ping Pong mechanism. Data for *Lm*TDPX1 are from [13] and were fitted to the Michaelis–Menten equation for a Ping Pong mechanism.

TDPX	k_{cat} (s^{-1})	$K_{m,CuOOH}$ (μM)	$K_{m,TryX}$ (μM)	$10^5 \times k_{1,CuOOH}$ ($M^{-1} \cdot s^{-1}$)	$k_{2,TryX}$ ($M^{-1} \cdot s^{-1}$)
*Tb*TDPX2*	38.3 ± 9.2	346 ± 88	69 ± 18	1.1†	5.6†
*Tb*TDPX2‡	17.3 ± 3.8	80§	25§	2.2 ± 0.2	6.9 ± 0.5
*Tb*TDPX3	∞	∞	∞	1.0	2.1
*Lm*TDPX1	16.2	207	2.6	0.79	62

* Data from Figure 2 were globally fitted by non-linear regression using proportional weighting to the equation describing a Ping Pong mechanism.

† Calculated from k_{cat}/K_m values.

‡ Data from Supplementary Figure S2 were analysed using the integrated Dalziel rate equation describing a Ping Pong mechanism; results are weighted means for two independent experiments.

§ Calculated from $K_m = k_{cat}/k$.

Figure 3 Ribbon diagram of *Tb*TDPX2 with secondary-structure elements labelled

α-Helices are coloured magenta, β-strands are coloured cyan and 3_{10}-helices (θ1 and θ2) are shown in green. The peroxidatic and resolving cysteine side chains are shown as sticks. See the text for further details.

residues are all conserved in the GPX family, except Tyr[41], which is specific to *Tb*TDPX2. The Cys[39] Sγ atom accepts a hydrogen bond from the Tyr[41] N atom (3.2 Å) and is 3.5 Å from the Trp[129] Nε1 atom, 3.4 Å from the Asn[130] Nδ2 atom and 3.9 Å from the Gln[74] Oε1 atom. A water molecule sits 3.4 Å from the Cys[39] Sγ atom on the surface of *Tb*TDPX2. The Cys[39] N atom hydrogen-bonds to the Thr[42] OH group, which is conserved in TDPXs and GPXs. It is not essential for catalysis [11], but appears to stabilize the active-site structure. Both Ala[36] and Tyr[41] are situated on the same loop (β3–α1) as Cys[39]. Analysis of a surface-charge

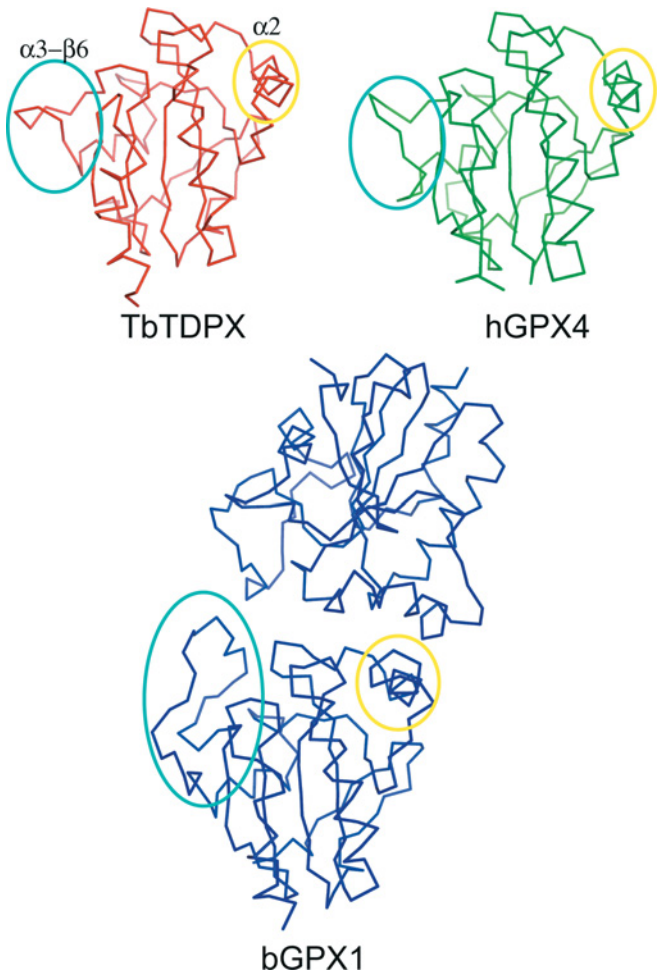

Figure 4 Cα backbone representations of *Tb*TDPX2, human GPX4 and bovine GPX1

Circled in yellow is helix α2 from each structure, showing the similarity between the monomeric *Tb*TDPX2 and human GPX4 (hGPX4) and their difference from bovine GPX1 (bGPX1). Circled in blue is the loop α3–β6, which is the same length in hGPX4, though taking on a slightly different conformation, and markedly different in bGPX1. This loop is involved in dimer interface interactions in the oligomeric GPXs and may also regulate substrate specificity.

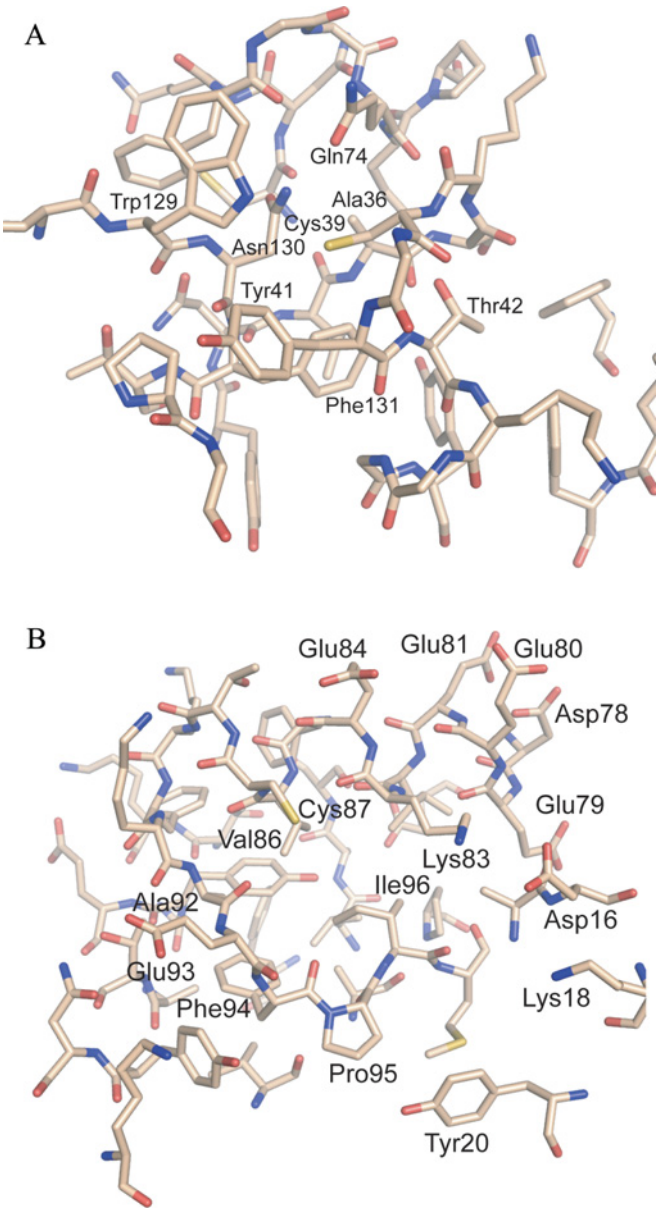

Figure 5 Detailed stick representation of (A) the peroxidatic cysteine and (B) the resolving cysteine environments

Important residues have been labelled and are discussed in the text. Oxygen atoms are depicted in red, nitrogen atoms in blue, sulphur atoms in yellow and carbon atoms in cream.

representation (Figure 6, left-hand panel) shows that the active-site region around Cys[39] is not a well-defined pocket or cleft. However, it lies in a predominantly positively charged region of the protein that may influence its substrate specificity.

The resolving Cys[87] is situated at the C-terminus of helix α2. It lies on the surface of the protein, is solvent-accessible and is situated at one end of a distinct pocket which is 14 Å long and 10 Å wide (Figure 6, right-hand panel). The base of the pocket is lined by residues Tyr[20], Pro[95] and Ile[96], with Val[86] immediately below Cys[87] (Figure 5B). Down one side are the charged side chains of Lys[18], Asp[16] and Lys[83]. The opposite side is lined by main-chain atoms of Ala[92], Glu[93] and Phe[94], and a negatively charged patch of Asp[78], Glu[79], Glu[80], Glu[81] and Glu[84] is seen on the electrostatic surface representation immediately above the charged side of the pocket. Cys[87] does not interact directly with other residues in *Tb*TDPX2 in the reduced state. This is particularly unusual, as it is situated in an α-helix, and although neighbouring residues follow the normal hydrogen-bonding pattern seen in such helices, Cys[87] appears to remain non-bonded and flexible, suggesting its prerequisite for movement.

Possible mechanism and druggability

TDPXs are predicted to undergo significant conformational changes between their respective reduced and oxidized structures [11,13], as observed for *Pt*GPX5 [15]. A model based on oxidized *Pt*GPX5 (Figure 7) suggests that α2 must completely unravel, causing loop β4–α2 to bulge outwards and allowing Cys[87] to travel some 12 Å to form a disulphide bond with Cys[39], which has itself moved 10 Å on the flexible β3–α11 loop. The trigger for this conformational change, which must reside in conversion of the Cys[39] thiolate group into a sulphenate group, merits further investigation. These complex structural changes could explain the finite Ping Pong mechanism found here by kinetic analysis (Figure 2 and Supplementary Figure S2) in contrast with the

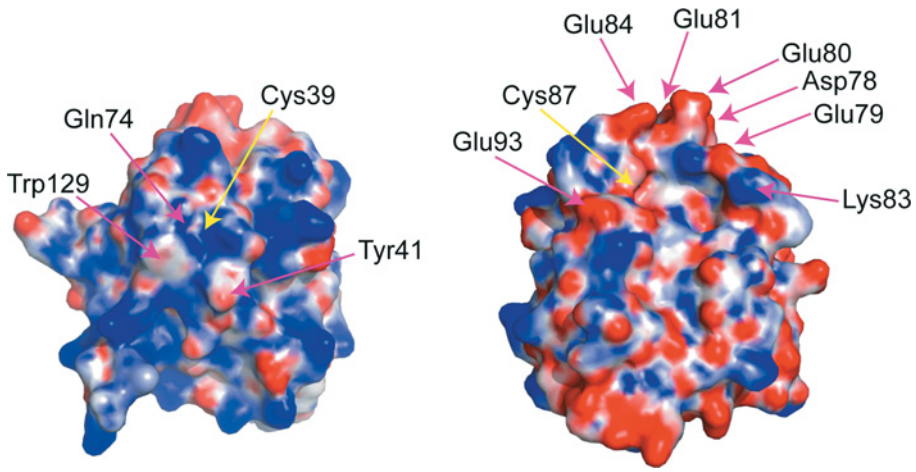

Figure 6 Surface electrostatic potential representation of *Tb*TDPX2

Positive charge is shown as blue and negative charge as red. The left-hand panel shows the positively charged region surrounding the peroxidatic Cys[39] with other residues marked as a guide to orient with other Figures. The right-hand panel shows the enzyme rotated 90° along the *y*-axis to reveal the environment surrounding the resolving Cys[87]. The pocket below Cys[87] can clearly be seen, as can the negatively charged glutamate-rich region above the pocket.

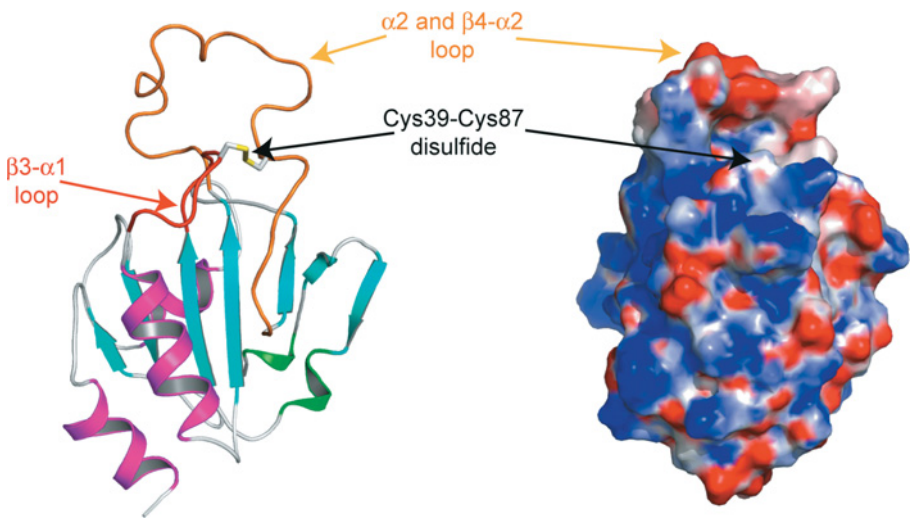

Figure 7 Ribbon and surface potential representations of the model of oxidized *Tb*TDPX2 based on *Pt*GPX5

In the ribbon diagram, the loop containing Cys[39] is coloured red, that containing Cys[87] is orange and the disulphide between the two cysteine residue is shown as sticks. The electrostatic surface representation shows the position of the disulphide and how the structural changes associated with oxidation generate surface features that may be of value in the design of enzyme inhibitors, for example the deep pocket created immediately above the disulphide bond, the base of which is lined by Phe[85], with a negatively charged lid of Glu[80] and Glu[81].

selenium type of glutathione peroxidases, which lack the resolving cysteine residue and display an infinite k_{cat}.

Although the peroxidative Cys[39] occupies a rather flat featureless surface in the reduced form, the environment of Cys[87] forms a defined pocket that could be exploited for drug design (Figure 6). Likewise the model of the oxidized form predicts a deep pocket immediately above the disulphide bond (Figure 7). Both forms therefore present potentially druggable sites for small-molecule inhibition. Structural studies on the oxidized form of *Tb*TDPX2 are necessary to confirm this prediction.

We thank Dr Paul Fyfe and Dr Scott Cameron for crystallographic data collection at the European Synchrotron Radiation Facility. This work is supported by the Wellcome Trust (grant nos. WT 079838 and WT 083481).

REFERENCES

1 Stuart, K. D., Brun, R., Croft, S. L., Fairlamb, A. H., Gurtler, R. E., McKerrow, J. H., Reed, S. and Tarleton, R. L. (2008) Kinetoplastids: related protozoan pathogens, different diseases. J. Clin. Invest. **118**, 1301–1310
2 Fairlamb, A. H. (2003) Chemotherapy of human African trypanosomiasis: current and future prospects. Trends Parasitol. **19**, 488–494
3 Fairlamb, A. H. and Cerami, A. (1985) Identification of a novel, thiol-containing co-factor essential for glutathione reductase enzyme activity in trypanosomatids. Mol. Biochem. Parasitol. **14**, 187–198
4 Krieger, S., Schwarz, W., Ariyanayagam, M. R., Fairlamb, A. H., Krauth-Siegel, R. L. and Clayton, C. (2000) Trypanosomes lacking trypanothione reductase are avirulent and show increased sensitivity to oxidative stress. Mol. Microbiol. **35**, 542–552
5 Ariyanayagam, M. R., Oza, S. L., Guther, M. L. and Fairlamb, A. H. (2005) Phenotypic analysis of trypanothione synthetase knockdown in the African trypanosome. Biochem. J. **391**, 425–432

6 Comini, M. A., Guerrero, S. A., Haile, S., Menge, U., Lunsdorf, H. and Flohé, L. (2004) Validation of *Trypanosoma brucei* trypanothione synthetase as drug target. Free Radical Biol. Med. **36**, 1289–1302

7 Comini, M. A., Krauth-Siegel, R. L. and Flohé, L. (2007) Depletion of the thioredoxin homologue tryparedoxin impairs antioxidative defence in African trypanosomes. Biochem. J. **402**, 43–49

8 Wilkinson, S. R., Horn, D., Prathalingam, S. R. and Kelly, J. M. (2003) RNA interference identifies two hydroperoxide metabolizing enzymes that are essential to the bloodstream form of the African trypanosome. J. Biol. Chem. **278**, 31640–31646

9 Hillebrand, H., Schmidt, A. and Krauth-Siegel, R. L. (2003) A second class of peroxidases linked to the trypanothione metabolism. J. Biol. Chem. **278**, 6809–6815

10 Schlecker, T., Schmidt, A., Dirdjaja, N., Voncken, F., Clayton, C. and Krauth-Siegel, R. L. (2005) Substrate specificity, localization, and essential role of the glutathione peroxidase-type tryparedoxin peroxidases in *Trypanosoma brucei*. J. Biol. Chem. **280**, 14385–14394

11 Schlecker, T., Comini, M. A., Melchers, J., Ruppert, T. and Krauth-Siegel, R. L. (2007) Catalytic mechanism of the glutathione peroxidase-type tryparedoxin peroxidase of *Trypanosoma brucei*. Biochem. J. **405**, 445–454

12 Wilkinson, S. R., Meyer, D. J., Taylor, M. C., Bromley, E. V., Miles, M. A. and Kelly, J. M. (2002) The *Trypanosoma cruzi* enzyme TcGPXI is a glycosomal peroxidase and can be linked to trypanothione reduction by glutathione or tryparedoxin. J. Biol. Chem. **277**, 17062–17071

13 König, J. and Fairlamb, A. H. (2007) A comparative study of type I and type II tryparedoxin peroxidases in *Leishmania major*. FEBS J. **274**, 5643–5658

14 Kabsch, W. (1993) Automatic processing of rotation diffraction data from crystals of initially unknown symmetry and cell constants. J. Appl. Crystallogr. **26**, 795–800

15 Koh, C. S., Didierjean, C., Navrot, N., Panjikar, S., Mulliert, G., Rouhier, N., Jacquot, J. P., Aubry, A., Shawkataly, O. and Corbier, C. (2007) Crystal structures of a poplar thioredoxin peroxidase that exhibits the structure of glutathione peroxidases: Insights into redox-driven conformational changes. J. Mol. Biol. **370**, 512–529

16 Vagin, A. and Teplyakov, A. (1997) MOLREP: an automated program for molecular replacement. J. Appl. Crystallogr. **30**, 1022–1025

17 Collaborative Computational Project, Number 4 (1994) The CCP4 suite: programs for protein crystallography. Acta Crystallogr. Sect. D Biol. Crystallogr. **50**, 760–763

18 Murshodov, G. (1997) Refinement of macromolecular structures by the maximum-likelihood method. Acta Crystallogr. D **53**, 240–255

19 Emsley, P. and Cowtan, K. (2004) Coot: model-building tools for molecular graphics. Acta Crystallogr. D **60**, 2126–2132

20 Dolinsky, T. J., Nielsen, J. E., McCammon, J. A. and Baker, N. A. (2004) PDB2PQR: an automated pipeline for the setup of Poisson–Boltzmann electrostatics calculations. Nucleic Acids Res. **32**, W665–W667

21 Baker, N. A., Sept, D., Joseph, S., Holst, M. J. and McCammon, J. A. (2001) Electrostatics of nanosystems: application to microtubules and the ribosome. Proc. Natl. Acad Sci. U.S.A. **98**, 10037–10041

22 Holm, L. and Sander, C. (1996) Mapping the protein universe. Science **273**, 595–603

23 Epp, O., Ladenstein, R. and Wendel, A. (1983) The refined structure of the selenoenzyme glutathione peroxidase at 0.2 nm resolution. Eur. J. Biochem. **133**, 51–69

24 Kleywegt, G. J. and Jones, T. A. (1995) Where freedom is given, liberties are taken. Structure **3**, 535–540

25 Schwede, T., Kopp, J., Guex, N. and Peitsch, M. C. (2003) SWISS-MODEL: an automated protein homology-modelling server. Nucleic Acids Res. **31**, 3381–3385

26 Martin, J. L. (1995) Thioredoxin – a fold for all reasons. Structure **3**, 245–250

27 Qi, Y. and Grishin, N. V. (2005) Structural classification of thioredoxin-like fold proteins. Proteins **58**, 376–388

28 Scheerer, P., Borchert, A., Krauss, N., Wessner, H., Gerth, C., Hohne, W. and Kuhn, H. (2007) Structural basis for catalytic activity and enzyme polymerization of phospholipid hydroperoxide glutathione peroxidase-4 (GPx4). Biochemistry **46**, 9041–9049

Received 2 May 2008/2 June 2008; accepted 4 June 2008
Published as BJ Immediate Publication 4 June 2008, doi:10.1042/BJ20080889

Biochem. J. (2008) **414**, 375–381 (Printed in Great Britain) doi:10.1042/BJ20080889

online data

SUPPLEMENTARY ONLINE DATA

Structural and mechanistic insights into type II trypanosomatid tryparedoxin-dependent peroxidases

Magnus S. ALPHEY[1], Janine KÖNIG[1] and Alan H. FAIRLAMB[2]

Division of Biological Chemistry and Drug Discovery, College of Life Sciences, University of Dundee, Dundee DD1 5EH, Scotland, U.K.

Table S1 Data collection and refinement statistics for *Tb*TDPX2

Numbers in parentheses represent the highest resolution bin of width approx. 0.06 Å.

Parameter	Value
Space group	$P2_1$
Cell dimensions	
a	43.3 Å
b	32.7 Å
c	58.3 Å
β	95.9°
X	
Resolution (Å)	58.0–2.1
Observed reflections	37396
Unique reflections	9469
Wilson *B* (Å^2)	27.3
Completeness (%)	96.2 (78.5)
Multiplicity	3.9 (2.7)
R_{merge} (%)	5.9 (26.0)
$\langle I/\sigma(I)\rangle$	25.5 (12.2)
R_{work} (%)	20.5 (23.2)
R_{free} (%)	26.3 (24.9)
r.m.s.d. from ideal values	
Bond lengths (Å)	0.008
Bond angles (°)	1.114
B factors (Å^2)	
Overall	27.7
Main chain	27.2
Side chain	28.1
Waters	31.5
Residues in most favourable regions (%)	92.1
Residues in additional allowed regions (%)	7.9

[1] These authors contributed equally to this work.

[2] To whom correspondence should be addressed (email a.h.fairlamb@dundee.ac.uk).

The model co-ordinates and structure factors have been deposited with the RSCB PDB (Research Collaboratory for Structural Bioinformatics Protein Data Bank) under the accession code 2VUP.

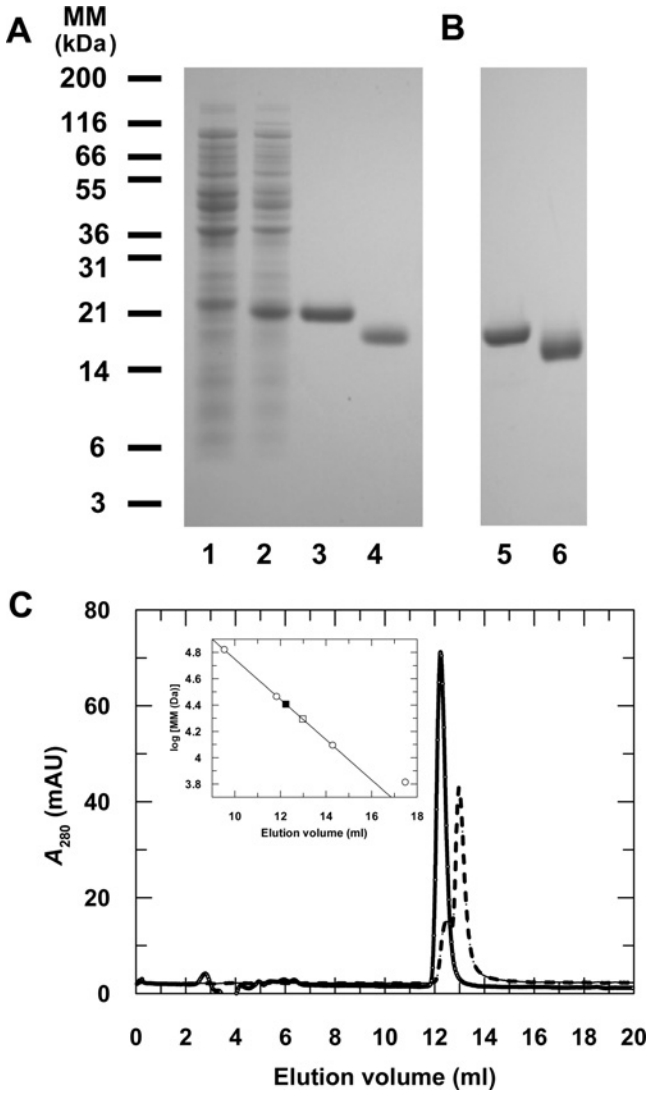

Figure S1 Purification of recombinant *Tb*TDPX2 from *E. coli*

(**A**) SDS/PAGE analysis: lane 1, uninduced fraction of BL21 Star (DE3) pLysS (pET-15b-TbTDPX2); lane 2, 4 h after induction with isopropyl β-D-thiogalactopyranoside; lane 3, 2 μg of purified His_6-tagged protein; lane 4, 2 μg of non-tagged *Tb*TDPX2. Abbreviation: MM, molecular mass. (**B**) SDS/12%-(w/v)-NuPAGE analysis: lane 5, 2 μg of non-tagged reduced *Tb*TDPX2 (50 mM dithiothreitol); lane 6, 2 μg of non-tagged oxidised *Tb*TDPX2 (5-fold molar excess of H_2O_2). The redox state was maintained with 100 mM iodoacetamide. (**C**) Size-exclusion chromatography of reduced and oxidized *Tb*TDPX2 on Superdex 75 10/300 GL. Broken line, *Tb*TDPX2 reduced with 50 mM dithiothreitol; continuous line, *Tb*TDPX2 oxidized with a 5-fold molar excess of H_2O_2. The inset shows a plot of elution volume versus log (molecular mass) in Da {log [MM (Da)]} of low-molecular-mass standards (Sigma–Aldrich; albumin, 66000 Da; carbonic anhydrase, 29000 Da; cytochrome c, 12400 Da; aprotinin, 6500 Da). The predicted molecular mass of the *Tb*TDPX2 monomer is 19168 Da. The elution volume of the reduced protein is represented by □ (molecular mass 19600 Da) and the oxidized protein by ■ (molecular mass 25 400 Da). Abbreviation: mAU, milli-absorbance unit.

Received 2 May 2008/2 June 2008; accepted 4 June 2008
Published as BJ Immediate Publication 4 June 2008, doi:10.1042/BJ20080889

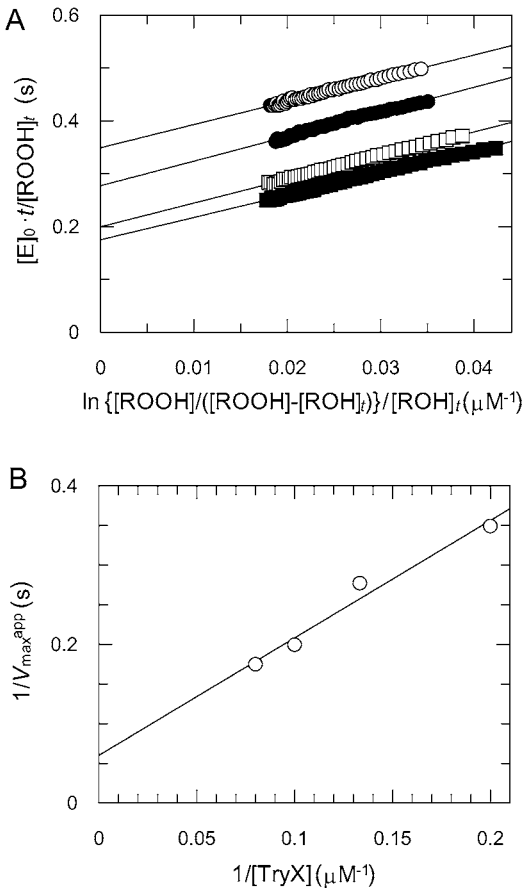

Figure S2 Kinetic properties of *Tb*TDPX2 analysed by the integrated Dalziel rate equation

Kinetic properties of *Tb*TDPX2 were analysed by progress-curve analysis using the integrated Dalziel rate equation for a two-substrate reaction. (**A**) The peroxidase activity of *Tb*TDPX2 was determined with 75 μM cumene hydroperoxide and various concentrations of TryX (○, 5 μM; ●, 7.5 μM; □, 10 μM; ■, 12.5 μM). The slope corresponds to $\varphi 1$, the reciprocal of the rate constant, k_1, for cumene hydroperoxide. $[E]_0$ is initial enzyme concentration, and t is time. (**B**) Secondary plot of the reciprocal apparent V_{max} data, calculated from the intercepts of the first plot, against the reciprocal TryX concentrations. The slope corresponds to $\varphi 2$, the reciprocal of rate constant, k_2, for TryX, and the ordinate intercept corresponds to $\varphi 0$, the reciprocal of the catalytic-centre activity, k_{cat}. Kinetic constants are reported in Table 1 of the main paper.